Research Square

Preprints are preliminary reports that have not undergone peer review.
They should not be considered conclusive, used to inform clinical practice,
or referenced by the media as validated information.

Construction and validation of predictive model of ankle joint muscle tone hyperactivity in cerebral palsy patients based on radiomics

Maimaiti Abulimiti
Second Affiliated Hospital of Xinjiang Medical University
Chunyu Zhang
Henan Medical University
Baofeng Yan
Wyyanbaofeng@163.com

Second Affiliated Hospital of Xinjiang Medical University

Research Article

Keywords: Cerebral palsy, Radiomics, Ankle joint muscle tone, Predictive model

Posted Date: November 25th, 2026

DOI: https://doi.org/10.21203/rs.3.rs-11582857/v1

License: This work is licensed under a Creative Commons Attribution 4.0 International License.
Read Full License

Additional Declarations: No competing interests reported.

Construction and validation of predictive model of ankle joint muscle tone hyperactivity in cerebral palsy patients based on radiomics

Authors:Maimaiti Abulimiti[1], Chunyu Zhang[1], Baofeng Yan[2]
Corresponding author：Baofeng Yan，E-mail：Wyyanbaofeng@163.com
Maimaiti Abulimiti and Chunyu Zhang contributed equally to this manuscript, and should be considered co-first authors.

Maimaiti Abulimiti, male, Candidate of master's degree, Department of Neurosurgery,The Second Affiliated Hospital of Xinjiang Medical University, Xinjiang, China. E-mail:2825176472@qq.com.

Chunyu Zhang, male, The First Affiliated Hospital of Henan Medical University, Henan, China.E-mail: zhangchunyu5033@outlook.com.

Baofeng Yan, male, Department of Neurosurgery,The Second Affiliated Hospital of Xinjiang Medical University, Xin jiang, China. E-mail: Wyyanbaofeng@163.com.

Funding Information: This article was supported by “Tianshan Talents”medical and health high-level talent training plan（TSYC202401B081）

Abstract

Background: Currently, no studies have been conducted using radiomics to predict cerebral palsy. Therefore, this study aims to extract and analyze the radiomics features of the head MRI of patients with cerebral palsy, screen out the key radiomics features related to the muscle tone hyperactivity of the left and right ankle joints, and construct a predictive model, with the expectation of providing new imaging evidence for the early diagnosis and precise intervention of ankle muscle tone hyperactivity in patients with cerebral palsy. **Methods:** Retrospectively collected case and imaging data of 296 cerebral palsy (CP) patients treated in the Department of Neurosurgery at the Second Affiliated Hospital of Xinjiang Medical University from January 2022 to September 2025, 221 cases were ultimately included based on inclusion and exclusion criteria. The dataset was randomly divided into a training set (154 cases) and a validation set (67 cases) at a ratio of 7:3. Radiomic features for each brain region were extracted from each CP patient. Features were screened through Z-score normalization, Spearman correlation analysis, feature de-duplication, and Lasso regression with L1 regularization. A random forest model was selected to establish the predictive model. **Results:** Each cerebral palsy patient has 162 brain regions, with 100 imaging radiomics features extracted from each region, totaling 162*100=16,200 features. Among these, 46 features were identified as associated with muscle tone hyperactivity in the left ankle joint, and 36 features were associated with muscle tone hyperactivity in the right ankle joint. The top 10 optimal features were selected to establish a predictive model. The Area Under the Curve (AUC) values for the left ankle joint training set and validation set were 0.978 and 0.631, respectively, while those for the right ankle joint training set and validation set were 0.970 and 0.649, respectively. **Conclusion:** The following features were identified as significant predictors for left ankle joint muscle tone hyperactivity: elogation of the right retrolenticular part of internal capsule, normalized gray level non-uniformity in the left retrolenticular part of internal capsule, cluster prominence of the left posterior thalamic radiation(including optic radiation), maximum probability in the right occipital pole, and sphericity in the anterior part of the right middle temporal gyrus. Conversely, flatness of left posterior superior temporal gyrus, least axis length in the right posterior superior temporal gyrus, and small-area low gray level emphasis in the left corticospinal tract were key predictors for right ankle joint muscle tone hyperactivity. The predictive model developed in this study exhibited overfitting tendencies, necessitating further optimization through multicenter, large-sample cohort studies.

Key words: Cerebral palsy; Radiomics; Ankle joint muscle tone; Predictive model

Introduction

cerebral palsy (CP) refers to a group of syndromes mainly characterized by motor disorders and postural abnormalities caused by non-progressive and permanent damage to the brain development of the fetus or infant, mainly due to cerebral ischemia and hypoxia[1]. It is the most common cause of childhood disability. Despite increased medical intervention, the incidence of CP remains stable at 1-2 per 1,000 live births[2][3][4]. Traditionally, the diagnosis of cerebral palsy has been based on signs of muscle tone hyperactivity and delayed development, which often leads to delay in diagnosis[5]. Therefore, early diagnosis is crucial for the treatment and prevention of cerebral palsy. Many studies have reported the predictive effectiveness of MRI and cranial ultrasound in the diagnosis of CP, MRI is generally regarded as a more sensitive imaging examination[6]. Tusor[7] et al. demonstrated that punctate white matter lesions detected by MRI in preterm infants were associated with changes in brain development and adverse motor outcomes. The advancements in magnetic resonance imaging (MRI) technology in recent decades have provided a unique opportunity to search for functional biomarkers of CP. Radiomics can transform existing medical imaging information into extractable data[8]. Radiomics marks a new research field, which will extract, process and analyze quantitative, high-throughput data to explore the relationship with valuable information[9]. Nie[10] et al. used a Deep-Learning method based on radiomics to predict the survival of high-grade gliomas, with an accuracy rate of 90.66%. For intracerebral hemorrhage (ICH), the radiomics model established by Xie [11]et al. demonstrated high accuracy in predicting early hematoma expansion in ICH patients.

Muscle tone hyperactivity in patients with cerebral palsy is a key factor affecting their motor function and quality of life. Clarifying the association between the radiomics characteristics of the head and muscle tone hyperactivity in patients with cerebral palsy may provide an important basis for early diagnosis and the formulation of personalized treatment plans. Currently, no studies have been conducted using radiomics to predict cerebral palsy. Therefore, this study aims to extract and analyze the radiomics features of the head MRI of patients with cerebral palsy, screen out the key radiomics features related to the muscle tone hyperactivity of the left and right ankle joints, and construct a predictive model, with the expectation of providing new imaging evidence for the early diagnosis and precise intervention of ankle muscle tone hyperactivity in patients with cerebral palsy. This lays a foundation for improving the prognosis of patients with cerebral palsy and enhancing their quality of life.

Methods

1. Participants

This study retrospectively collected 296 patients with cerebral palsy who were treated in the Department of Neurosurgery of the Second Affiliated Hospital of Xinjiang Medical University from January 2022 to September 2025. Among them, 178 were male and 118 were female, with an age of (10.8±3.69) years. There were 124 patients with mixed cerebral palsy, 150 patients with spastic cerebral palsy and 22patients with athetosis cerebral palsy. Inclusion criteria: Meeting the diagnostic criteria for cerebral palsy; The clinical data are complete; The magnetic resonance image data is complete and free of artifacts; There is no absence of brain structures in magnetic resonance images; The boundary between gray matter and white matter in the brain is clear. Exclusion criteria: Comorbid severe hydrocephalus, schizencephaly, and massive cerebral perforating malformation; There are brain trauma lesions, combined with secondary brain structural changes such as brain tumors and cerebral vascular malformations; Those who received botulinum toxin injection treatment, selective posterior rhizotomy(SPR), or orthopedic surgery within 6 months before enrollment; Accompanied by severe organ dysfunction; Those whose map registration quality does not meet the standards in image preprocessing.This study was approved by the Medical Ethics Committee of the Second Affiliated Hospital of Xinjiang Medical University (Approval No.2022H015), and the guardians of the pediatric patients signed the informed consent form.

2. Clinical and imaging data

The joint muscle tone grades of the bilateral elbow, wrist, knee and ankle joints of cerebral palsy patients were collected according to the modified Ashworth muscle tone Scale(MAS). The T1-weighted sagittal plane three-dimensional magnetization preparation rapid gradient echo (MPRAGE) sequences of the head of cerebral palsy patients were collected, covering the entire brain :128 layers, TR=2530ms, TE=3.39ms, layer thickness =1.33mm, inversion Angle =7°, inversion time =1100ms, FOV=256×256mm. The in-plane resolution =256×192.

3. Image preprocessing

Convert the data to NIFTI format using dcm2niix and view the image quality using MRIcroGL. ANTs kits (ANTsX/ANTs, https://github.com/ANTsX/ANTs) the standard Harvard - Oxford Atlas(HOA) and the Johns-Hopkins University (JHU) Atlas were registered to the individual structural space of each subject (Figure 1). This process mainly includes the following three steps:

(1) skull stripping was performed on the T1-weighted structural images of each subject to remove the non-target tissues outside the brain. This preprocessing step can effectively preserve the brain structural regions, reduce the interference of non-brain tissues on subsequent image registration, and thereby improve the accuracy and reliability of structural information.

(2) The brain images of each subject after skull stripping were registered to the standard MNI space through antsRegistrationSyN.sh. This step integrates linear and nonlinear registration strategies, aiming to precisely align the individual brain structure with the standard template and generate corresponding affine transformations and deformation field information for subsequent spatial transformations.

(3) By using the Ants Applied Transforms tool, the inverse transformations obtained in the above steps (including the inverse transformation of nonlinear deformation fields and the inverse transformation of affine matrices) are applied to the standard brain region map. Thus, the HOA atlas and the JHU atlas are mapped to the individual structural space of each subject. The individualized brain region masks obtained thereby can precisely correspond to the brain anatomical structure of each subject.By using the relevant tools in the SimpleITK library, N4 bias field correction was performed on the T1 structural images of all subjects, aiming to remove the low-frequency bias field in the images, making the image luminance distribution more uniform, and thereby improving the accuracy and reliability of subsequent analysis (Figure 2).

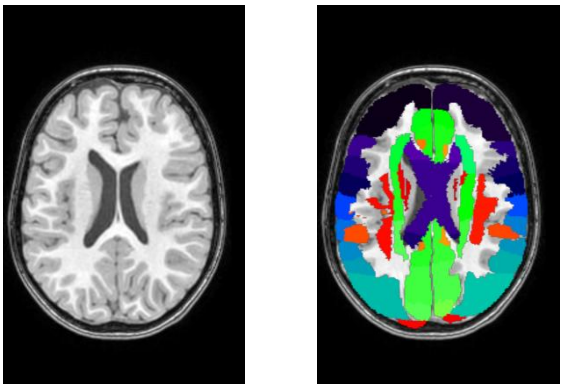

A **B**

Fig.1 Atlas registration to individual (A. Before registration, B. After registration)

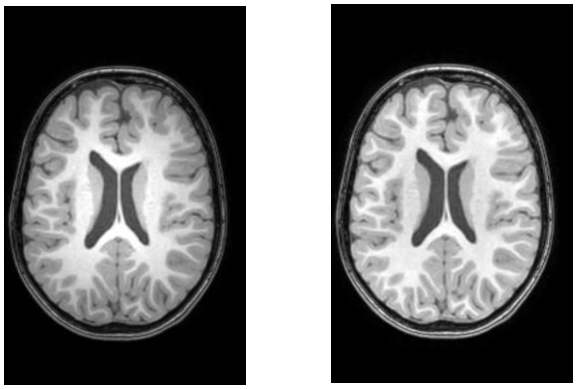

A **B**

Fig.2 N4 bias field correction(A. Before correction, B. After correction)

4. Radiomics feature extraction

The Radiomics features of each brain region of each cerebral palsy patient are extracted using the feature extractor of the Radiomics library. Before extracting the features, the number of T1 structures is resampled to 1mm*1mm*1mm. 100 radiomics features were extracted from each brain region, including 14 shape features, 18 firstorder statistical features, and 22 Gray-Level Co-occurrence Matrix (GLCM) features. 16 Gray-Level Run-Length Matrix (GLRLM) features, 16 Gray-Level Size Zone Matrix The GLSZM feature and 14 Gray-Level dependence Zone Matrix features (GLDM). Each cerebral palsy patient has 162 brain regions (112 HOA maps + 50 JHU maps), totaling 162*100= 16,200 features.

5. Feature screening

(1) Feature normalization: Perform Z-Score normalization on all features, scaling the feature values of the dataset to a mean of 0 and a standard deviation of 1.
(2) Feature screening based on Spearman correlation: An efficient initial screening strategy based on statistical correlation is adopted. By calculating the Spearman rank correlation coefficient between each feature and the target variable, the monotonic association strength between the feature and the predicted target is systematically evaluated. The screening process is arranged in descending order according to the absolute value of the correlation coefficient. A fixed proportion truncation method is used to retain the top 5% of the most relevant features, ensuring that the feature subset with the greatest predictive potential is retained while achieving rapid dimensionality reduction.
(3) Redundant feature screening: By constructing a feature correlation matrix system, highly correlated feature pairs are identified. A correlation threshold of 0.9 is adopted, combined with the retention principle of "survival of the fittest" - that is, for each pair of highly correlated features, the features that are more closely related to the target variable are retained first, and the relatively redundant features are removed to alleviate the problem of multicollinearity among features.
(4) Least Absolute Shrinkage and Selection Operator (LASSO) regularized feature screening: Utilizing the L1 regularization feature of LASSO regression to achieve automated feature selection. A 5-fold cross-validation is adopted to optimize within a wide logarithmic range of λ from 10^{-4} to 10^{1}, and the λ that minimizes the cross-validation error is selected as the optimal regularization parameter. This method can not only avoid the problem of overfitting, but also retain the feature subsets that make substantial contributions to the model prediction. Ultimately, the features with non-zero coefficients are retained and sorted by the absolute values of the coefficients. The top 10 most important features are selected for subsequent modeling.

6. Model construction and validation

Based on the absolute values of the LASSO regression coefficients, the top 10 best features were screened out, and the random forest algorithm was used to construct a prediction model for ankle muscle

tone hyperactivity. The parameters of the random forest are set as follows: the number of decision trees is 200, the maximum depth is 3, the minimum number of sample splits is 10, the minimum number of leaf node samples is 5, and balanced category weights are used to handle the problem of sample imbalance. The model validation adopted a random splitting method to divide the dataset into a training set and a test set in a 7:3 ratio, ensuring a balanced distribution of the two groups of data. All feature screening steps are only carried out on the training set, and the test set is only used for the performance evaluation of the final model. the model performance was evaluated using the Receiver Operating Curve (ROC) to calculate the Area Under the Curve (AUC) and its 95% confidence interval (obtained through 1000 Bootstrap self-help methods). And calculate the accuracy rate as an auxiliary evaluation index. The SHAP(SHapley Additive exPlanations) plot is adopted to interpret the model prediction results, quantify the contribution degree of each feature to model, and visually display the importance ranking of the features and their positive and negative influences on the prediction results through the SHAP plot.

7. Statistical methods

All statistical analyses in this study were conducted using Python3.9 software. Comparison of differences between clinical data groups: Continuous variables with normal distribution were expressed as "mean ± standard deviation", and independent sample t-tests were used; Continuous variables with non-normal distribution are expressed as the "median (interquartile range)". Radiomics feature screening employs a multi-stage strategy: Firstly, the top 5% features most strongly associated with the spasticity state are screened through the Spearman rank correlation coefficient. Secondly, the high collinearity redundant features are removed with a correlation threshold of 0.9 in combination with the "survival of the fittest" principle. Finally, the L1 regularization parameter of LASSO regression is optimized through 5-fold cross-validation to achieve zero feature weights for screening core features. A random forest prediction model was constructed based on the top 10 key features screened by LASSO. The ROC curve (AUC and 95% confidence interval were calculated through 1000 Bootstrap self-help methods) was used to evaluate the model's performance, and the contribution of each feature to the model's prediction was visualized through a SHAP graph. A P-value <0.05 is considered statistically significant.

Results

1. General Information

According to the inclusion and exclusion criteria, a total of 221 patients with cerebral palsy were finally included, including 133 males and 88 females, with an age of (10.7±3.09) years. Among them, there were 92 patients with mixed cerebral palsy, 110 patients with spastic cerebral palsy, and 19 patients with athetosis cerebral palsy. Among the left ankle joint muscle tension, 80 cases were normal and 140 cases were increased. Among the right ankle joint muscle tension, 68 cases were normal and 153 cases were increased. There were 62 cases with normal muscle tone in both the left and right ankle joints. There were 135 cases with increased muscle tone in both the left and right ankle joints. (Samples were collected according to the Ashworth Muscle Tone Scale. During statistical analysis, the data was changed to 0 for normal muscle tone and 1 for muscle tone hyperactivity as a binary variable.) They were randomly divided into a training set of 154 cases and a validation set of 67 cases at a ratio of 7:3 (Table 1).

Table1 Composition ratio of training and validation sets (n/%X±s)

Category	Training set(n=154)	Validation set(n=67)
age	10.8±3.24	10.6±2.73
Gender		
male	93(60.4)	40(59.7)
female	61(39.6)	27(40.3)
Muscle tone of the left ankle		
normal	56(36.4)	24(35.8)
hyperactivity	98(63.6)	43(64.2)

Category	Training set(n=154)	Validation set(n=67)
Muscle tone of the right ankle		
normal	51(33.1)	17(25.4)
hyperactivity	103(66.9)	50(74.6)

P >0.05

2. Results of feature screening

The same feature screening process was adopted for the left and right ankle joints: Firstly, from 16,200 radiomics features, 810 radiomics features related to muscle tone hyperactivity of the left and right ankle joints were respectively screened out using the Spearman correlation analysis method; Secondly, in the process of removing redundant features, no redundant features were screened out on either side. Finally, using the Lasso regression L1 regularization method, 46 radiomics features of the left ankle joint (Table 2) and 36 radiomics features of the right ankle joint (Table 3) were respectively screened out. The optimal alpha value of the left ankle joint is 0.0335, and that of the right ankle joint is 0.0423(Figures 3,4,5,6). The bar chart visualizes the weight of each feature (Figures 7 and 8).

Table2 The final selected radiomics features (left ankle)

Radiomic features	Coefficient
HOA_62_glszm_SmallAreaLowGrayLevelEmphasis	0.08428027
HOA_40_glszm_SmallAreaEmphasis	-0.072100856
HOA_22_shape_Sphericity	-0.067460387
JHU_22_glszm_GrayLevelNonUniformityNormalized	-0.040983341
JHU_30_glcm_ClusterProminence	-0.040259031
HOA_96_glcm_MaximumProbability	-0.039461667
JHU_30_glszm_SmallAreaLowGrayLevelEmphasis	-0.039398584
JHU_21_shape_Elongation	-0.034687992
HOA_3_shape_Elongation	0.031884638
JHU_16_shape_LeastAxisLength	0.029284059
HOA_59_glszm_LowGrayLevelZoneEmphasis	-0.025843601
JHU_32_glszm_GrayLevelNonUniformityNormalized	-0.025739391
HOA_50_shape_Flatness	0.025699381
HOA_46_glrlm_GrayLevelNonUniformityNormalized	-0.025335187
HOA_84_firstorder_Kurtosis	-0.024596154
HOA_108_glrlm_ShortRunLowGrayLevelEmphasis	0.022827323
JHU_42_gldm_DependenceNonUniformityNormalized	0.022585309
JHU_10_glszm_GrayLevelNonUniformity	0.022260792
HOA_46_glszm_GrayLevelNonUniformityNormalized	-0.02083564
JHU_8_gldm_LargeDependenceHighGrayLevelEmphasis	0.019247771
HOA_55_glrlm_LowGrayLevelRunEmphasis	0.019090934
HOA_101_gldm_LargeDependenceLowGrayLevelEmphasis	0.018757903
HOA_22_glszm_LargeAreaLowGrayLevelEmphasis	-0.016352951
JHU_41_shape_Sphericity	-0.014667912
HOA_48_shape_Elongation	0.013862855
HOA_39_shape_Sphericity	-0.013791241
JHU_45_glszm_SizeZoneNonUniformityNormalized	0.013143577
JHU_32_firstorder_Minimum	-0.01306539
HOA_53_glszm_SizeZoneNonUniformityNormalized	0.012465609
HOA_96_glszm_LargeAreaLowGrayLevelEmphasis	-0.011997305
HOA_27_glszm_LowGrayLevelZoneEmphasis	-0.011166928
HOA_32_glrlm_LongRunLowGrayLevelEmphasis	-0.008309239
HOA_46_glcm_JointEnergy	-0.006577371
HOA_7_shape_Flatness	0.006320314
HOA_7_shape_Elongation	0.006118813

Radiomic features	Coefficient
JHU_46_shape_Maximum2DDiameterRow	-0.00588834
HOA_25_glcm_Imc2	0.00490674
HOA_3_glszm_LargeAreaHighGrayLevelEmphasis	-0.004351011
JHU_25_glszm_GrayLevelNonUniformity	-0.004311572
HOA_22_glszm_SmallAreaEmphasis	0.003969394
HOA_93_shape_Flatness	-0.003589052
HOA_12_firstorder_Kurtosis	-0.00357204
HOA_21_shape_Sphericity	-0.002954032
HOA_38_firstorder_Kurtosis	-0.002734695
HOA_101_firstorder_Skewness	0.002621464
HOA_84_gldm_LargeDependenceHighGrayLevelEmphasis	-0.000793566

207

208 Table3 The final selected radiomics features (right ankle)

Radiomic features	Coefficient
HOA_20_shape_LeastAxisLength	-0.06805663
HOA_21_shape_Sphericity	-0.044977746
HOA_19_shape_Flatness	0.041843915
HOA_22_shape_Sphericity	-0.040659196
HOA_49_gldm_DependenceVariance	-0.029700969
HOA_48_shape_Elongation	0.028492324
JHU_20_glcm_Idmn	0.028225445
JHU_8_glszm_SmallAreaLowGrayLevelEmphasis	-0.026607889
HOA_3_shape_Elongation	0.025648994
HOA_25_gldm_DependenceEntropy	0.025074694
HOA_44_glszm_SmallAreaEmphasis	0.024988991
HOA_108_glszm_SmallAreaLowGrayLevelEmphasis	0.024636552
HOA_63_glcm_InverseVariance	-0.022482479
JHU_32_firstorder_Minimum	-0.021790119
HOA_80_firstorder_Minimum	-0.021233047
HOA_62_glrlm_LongRunHighGrayLevelEmphasis	-0.015949364
HOA_11_glcm_Idn	-0.014816655
JHU_22_glszm_GrayLevelNonUniformityNormalized	-0.013400329
HOA_46_firstorder_Uniformity	-0.01231994
HOA_101_glrlm_ShortRunLowGrayLevelEmphasis	0.01113332
HOA_46_glcm_ClusterProminence	0.009425167
JHU_44_glszm_SmallAreaLowGrayLevelEmphasis	-0.009107381
HOA_46_glcm_DifferenceVariance	0.008358812
JHU_30_firstorder_Minimum	-0.008276272
JHU_42_gldm_DependenceNonUniformityNormalized	0.008243116
JHU_8_glszm_LargeAreaLowGrayLevelEmphasis	-0.005167183
JHU_11_shape_Maximum2DDiameterColumn	-0.004445232
HOA_46_glcm_JointEnergy	-0.004297888
JHU_32_glszm_GrayLevelNonUniformityNormalized	-0.003976958
JHU_26_gldm_DependenceVariance	-0.003762242
JHU_21_glcm_Idmn	-0.003751676
HOA_25_shape_Elongation	-0.00254051
HOA_62_glcm_Idmn	-0.001401143
JHU_13_glcm_ClusterTendency	0.000592881
HOA_46_glszm_GrayLevelNonUniformityNormalized	-0.000265
HOA_50_shape_Flatness	0.000252808

Fig.3 Lasso cross-validation curve for the left ankle

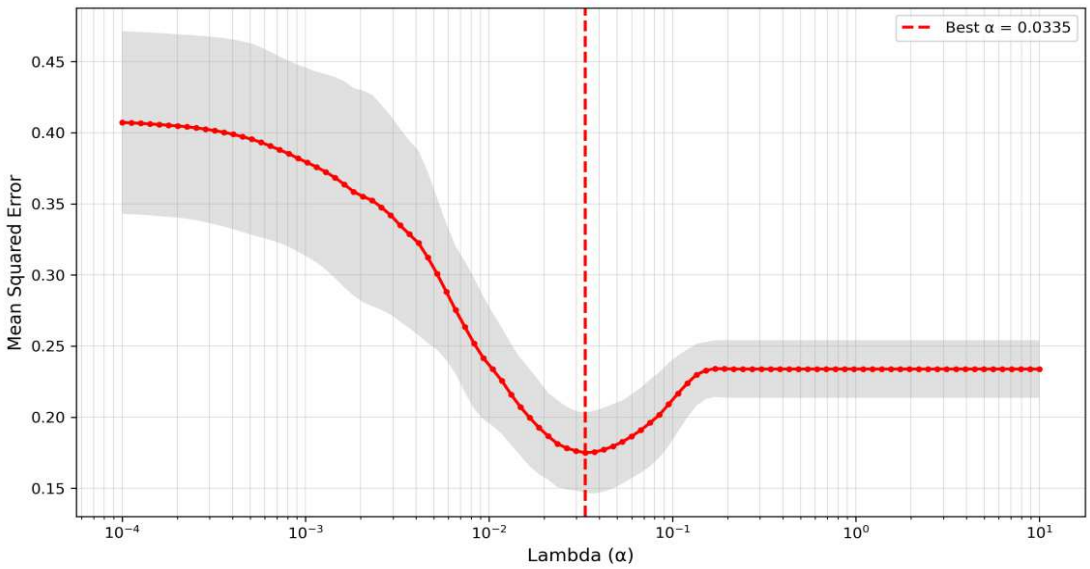

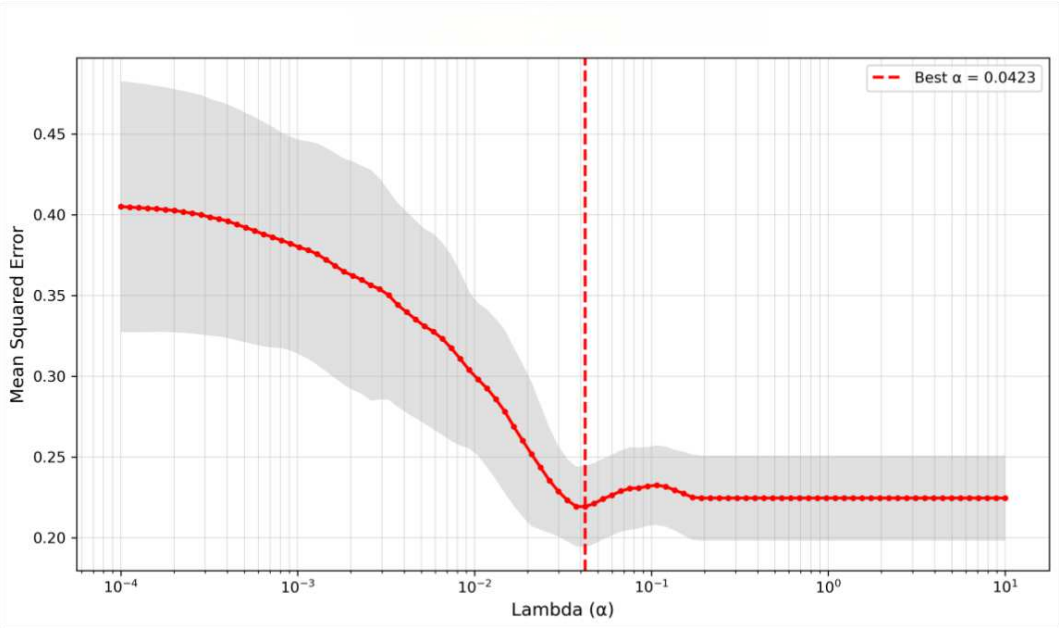

Fig.4 Lasso cross-validation curve for the right ankle

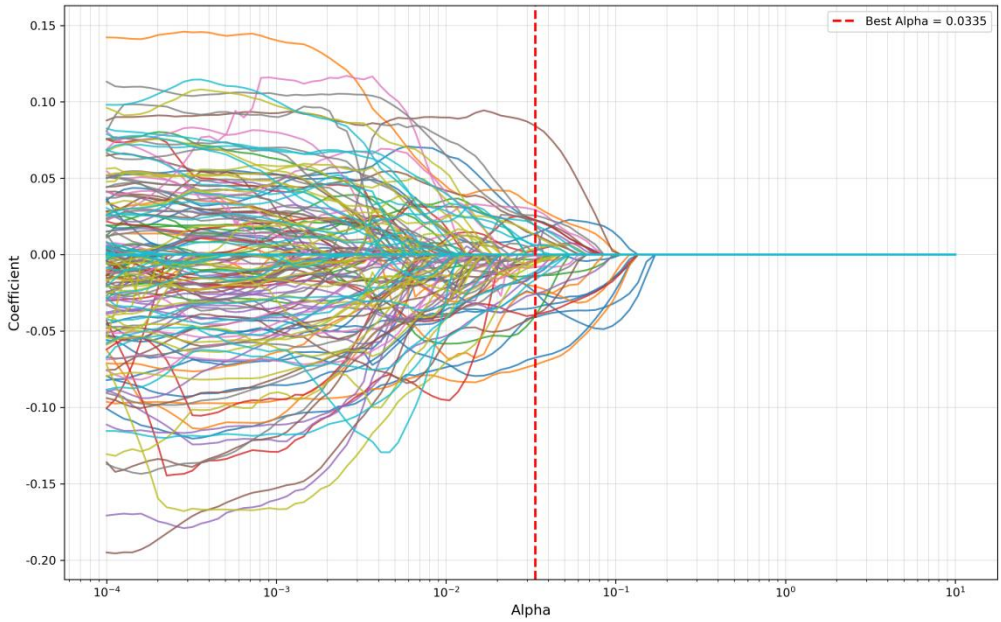

Fig.5 Lasso pathway diagram of the left ankle

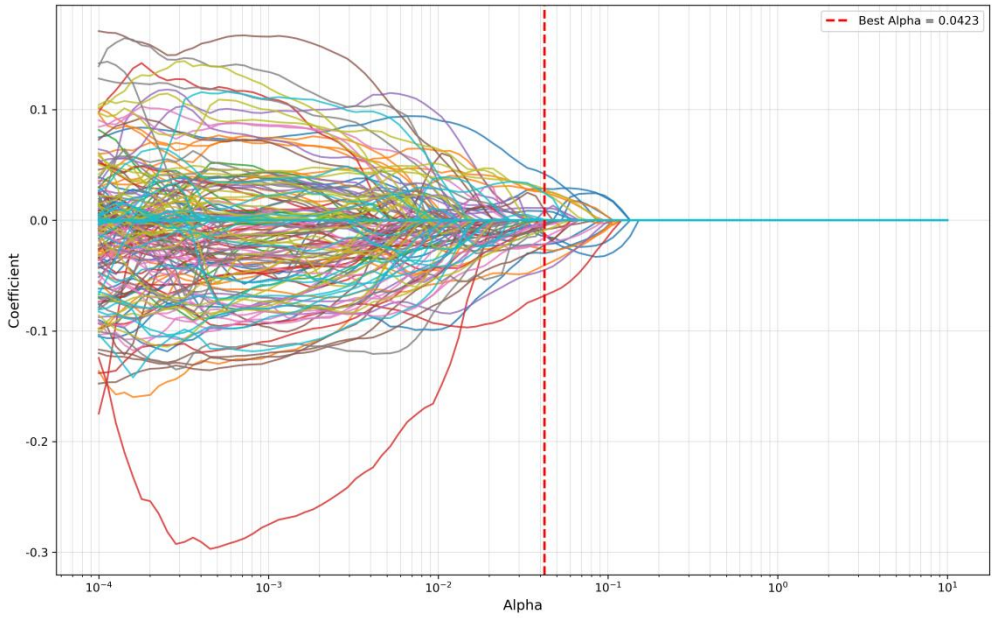

Fig.6 Lasso path diagram of the right ankle

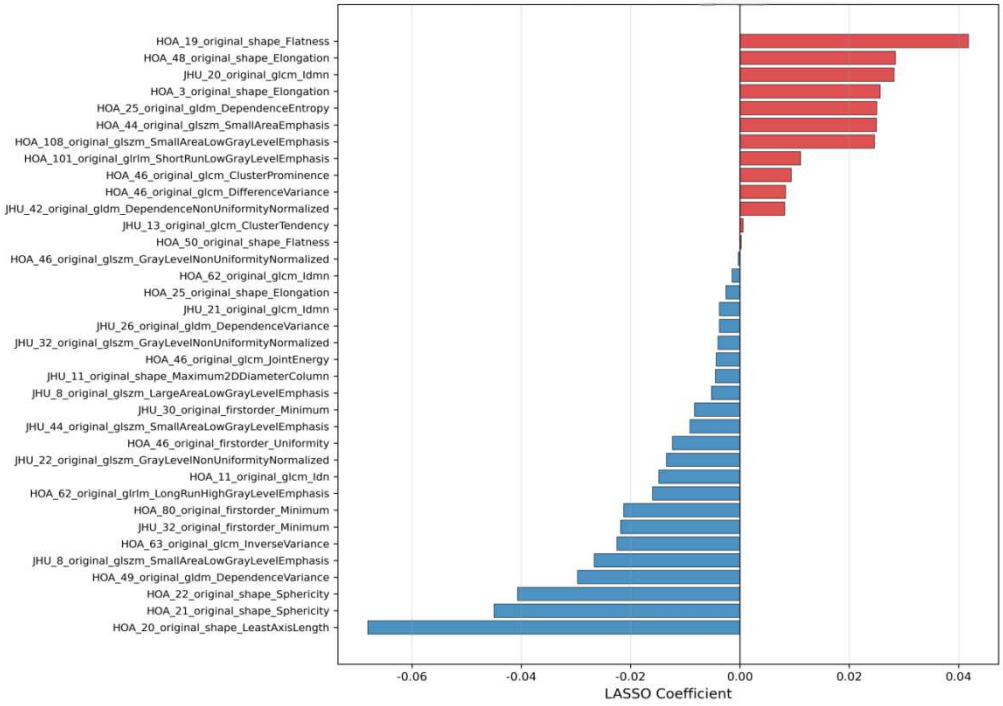

218

219 Fig.7 The final selected radiomics features (right ankle)

220

221

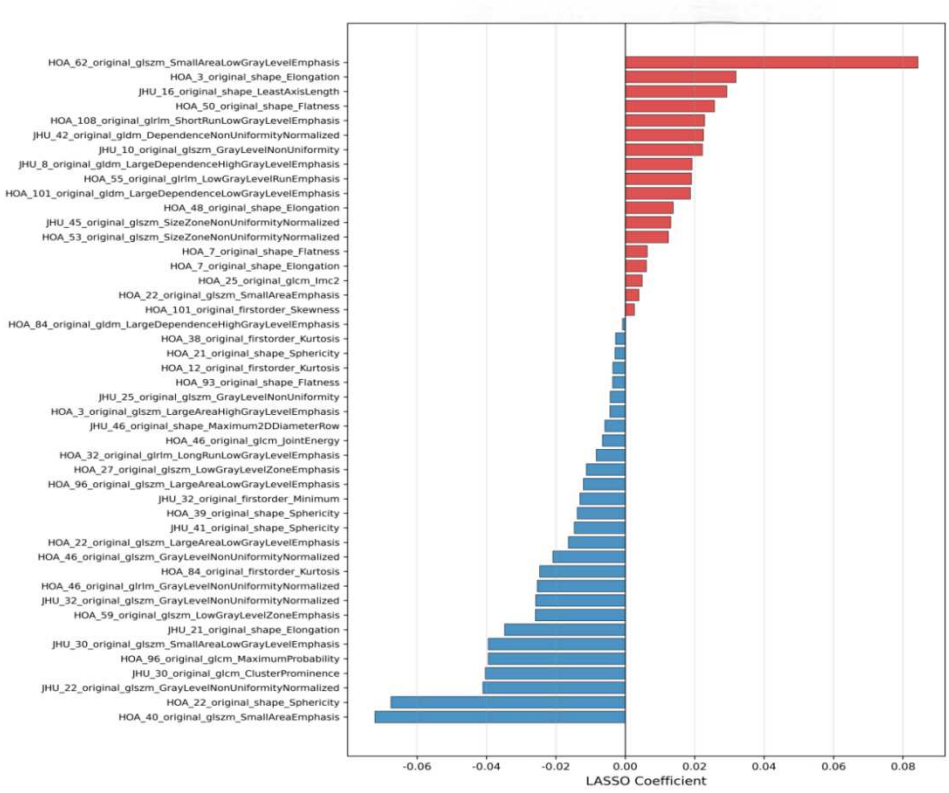

222

223 Fig.8 The final selected radiomics features (left ankle)

224 **3. Predictive model construction**

Based on the top 10 features screened out by Lasso (Tables 4 and 5), the Random Forest algorithm was used to construct a prediction model for muscle tone hyperactivity of ankle joint in patients with cerebral palsy.

Table4 Top 10 Features and Corresponding Brain Regions (Left Ankle)

Mark	Top 10 features	Corresponding brain regions
F1	HOA_62_glszm_SmallAreaLowGrayLevelEmphasis	Right Precuneous Cortex
F2	HOA_40_glszm_SmallAreaEmphasis	Right Supramarginal Gyrus posterior division
F3	HOA_22_shape_Sphericity	Right Middle Temporal Gyrus anterior division
F4	JHU_22_glszm_GrayLevelNonUniformityNormalized	Left Retrolenticular part of internal capsule
F5	JHU_30_glcm_ClusterProminence	Left Posterior thalamic radiation (include optic radiation)
F6	HOA_96_glcm_MaximumProbability	Right Occipital Pole
F7	JHU_30_glszm_SmallAreaLowGrayLevelEmphasis	Left Posterior thalamic radiation (include optic radiation)
F8	JHU_21_shape_Elongation	Right Retrolenticular part of internal capsule
F9	HOA_3_shape_Elongation	Left Insular Cortex
F10	JHU_16_shape_LeastAxisLength	Left Cerebral peduncle

Table5 Top 10 Features and Corresponding Brain Regions (Right Ankle)

Mark	Top 10 features	Corresponding brain regions
F1	HOA_20_shape_LeastAxisLength	Right Superior Temporal Gyrus posterior division
F2	HOA_21_shape_Sphericity	Left Middle Temporal Gyrus anterior division
F3	HOA_19_shape_Flatness	Left Superior Temporal Gyrus posterior division
F4	HOA_22_shape_Sphericity	Right Middle Temporal Gyrus anterior division
F5	HOA_49_gldm_DependenceVariance	Left Frontal Medial Cortex
F6	HOA_48_shape_Elongation	Right Intracalcarine Cortex
F7	JHU_20_glcm_Idmn	Left Posterior limb of internal capsule
F8	JHU_8_glszm_SmallAreaLowGrayLevelEmphasis	Left Corticospinal tract
F9	HOA_3_shape_Elongation	Left Insular Cortex
F10	HOA_25_gldm_DependenceEntropy	Left Middle Temporal Gyrus temporooccipital part

4. Model performance evaluation

The discriminative ability of the model was evaluated by using the ROC Curve, and the Area Under the Curve (AUC) and its 95% confidence interval were calculated. The AUC values of the training set and validation set of the left ankle joint were 0.978 and 0.631, respectively. The AUC values of the

training set and validation set of the right ankle joint were 0.970 and 0.649 respectively (Table 6). The 95% confidence interval of AUC was calculated by the Bootstrap method (1000 resampling). The ROC curves of the training set and the validation set were respectively plotted in the same coordinate system to visually compare the fitting degree and generalization ability of the models (Figures 9,10).

Table6 Compares the ROC curves of the training set and the validation set

	Training set				Validation set			
	AUC(95%CI)	Sensitivity	Specificity	Accuracy	AUC(95%CI)	Sensitivity	Specificity	Accuracy
R	0.978(0.954-0.995)	0.929	0.946	0.935	0.631(0.497-0.763)	0.442	0.958	0.627
L	0.970(0.943-0.988)	0.845	0.980	0.890	0.649(0.509-0.779)	0.300	1.000	0.478

P <0.001

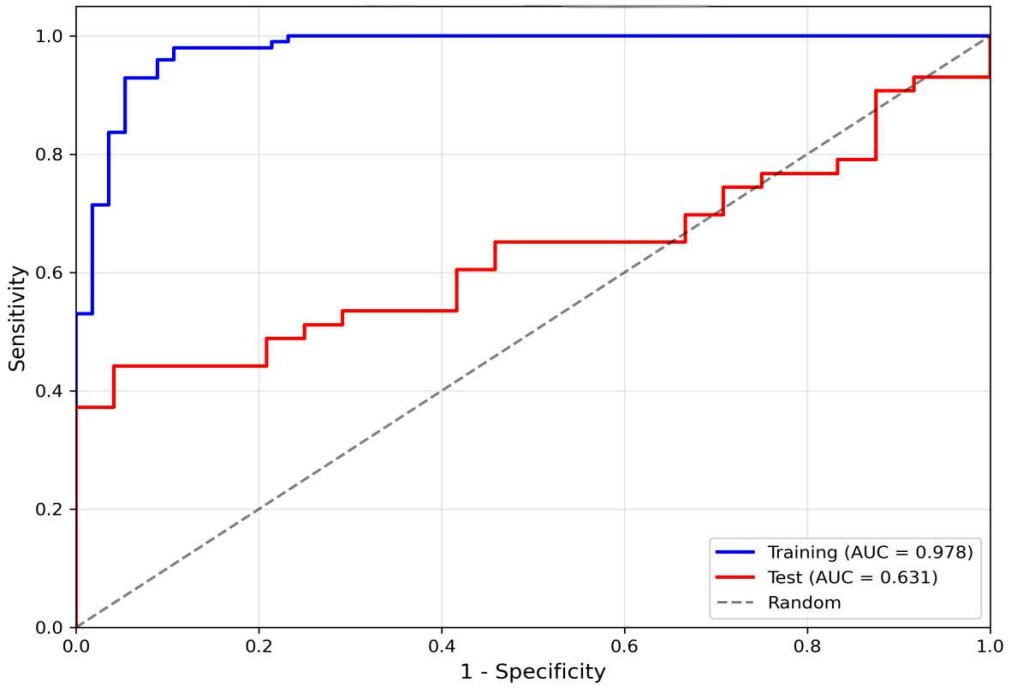

Fig.9 The ROC curves of the left ankle

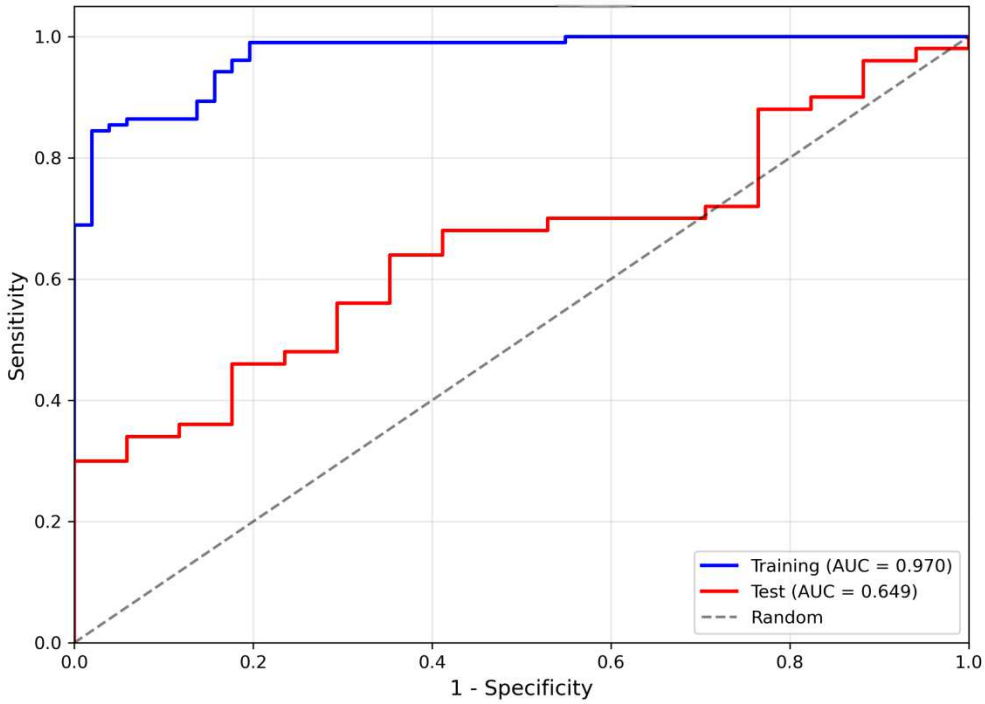

Fig.10 The ROC curves of the right ankle

5 SHAP plot analysis

Draw a SHAP plot to analyze the contribution degree of each feature to the model. The SHAP Summary Plot shows the distribution of SHAP values of all samples. Each point represents a sample, and the colors indicate the high or low characteristic values (red for high values and blue for low values). The position of the horizontal axis indicates the size of the SHAP values (positive values indicate a positive contribution to the positive prediction, and negative values indicate a negative contribution). It can be seen from the SHAP summary plot of the left ankle joint that: The five most important predictors in the left ankle model are the elongation of the right retrolenticular part of internal capsule (F8), the normalized gray level non-uniformity of the left retrolenticular part of internal capsule (F4), the cluster prominence of the left posterior thalamic radiation (include optic radiation) (F5), the maximum probability of the right occipital pole (F6), and the sphericity of the right middle temporal gyrus anterior division (F3), which contribute the vast majority of the predictive ability. All 10 features showed negative effects, that is, the lower these feature values were, the higher the probability of the model predicting positive left ankle muscle tone hyperactivity(Figure 11); It can be seen from the SHAP plot of the right ankle joint that the flatness of the left superior temporal gyrus posterior division (F3), the least axis length of the right superior temporal gyrus posterior division (F1), and the small area of low-gray-level emphasis of the left corticospinal tract (F8) are the three most important predictors in the right ankle model, contributing the most significant predictive ability. The first seven characteristics (F3, F1, F8, F10, F9, F5, F6) all show negative effects. The normalized inverse difference moment of the left posterior limb of the internal capsule(F7), the sphericity of the right middle temporal gyrus anterior division(F4) and the sphericity of the left middle temporal gyrus anterior division(F2) show positive effects, that is, the higher these characteristic values, the higher the probability predicted by the model as positive right ankle muscle tone (Figure 12). This is an important difference between the right ankle model and the left ankle model.

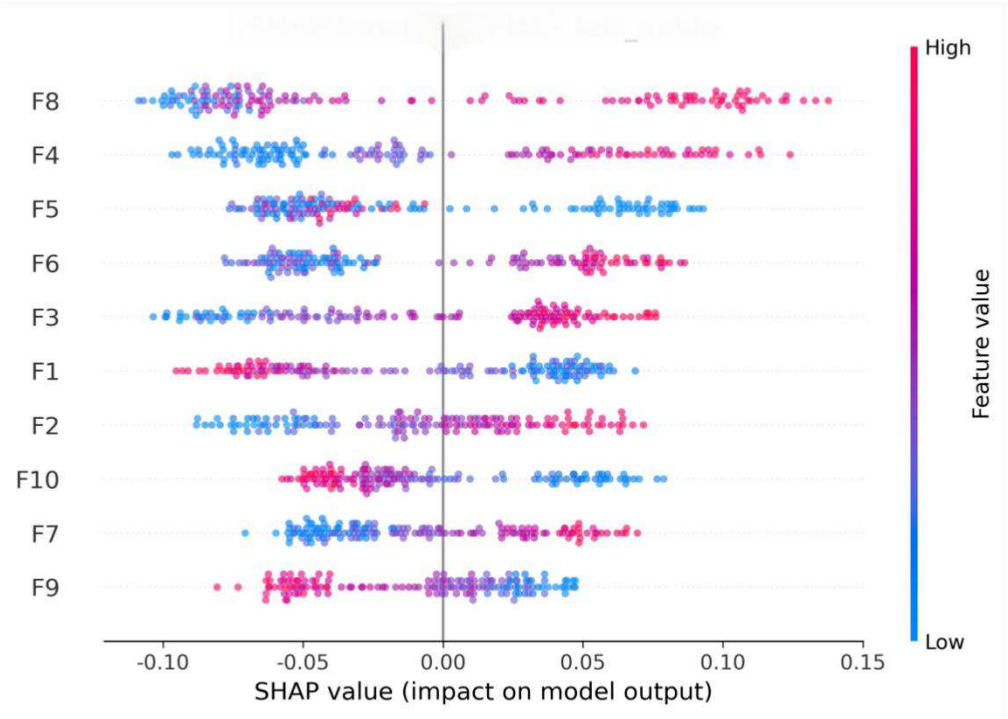

274

275 Fig.11 The SHAP plot of the left ankle

276

277

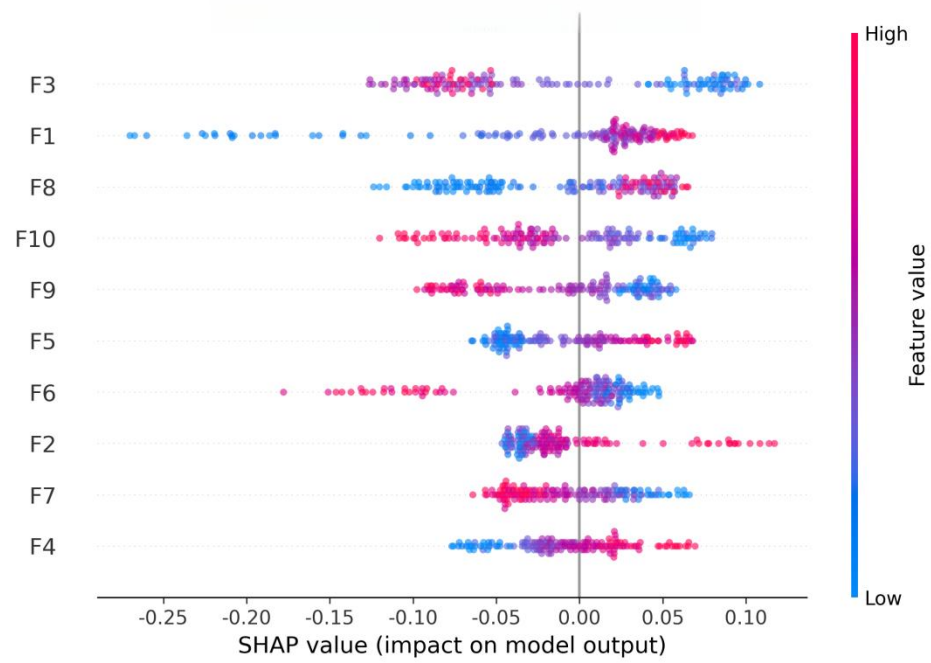

278

279 Fig.12 The SHAP plot of the right ankle

280

281

282

Discussion

Dystonia in patients with cerebral palsy is mainly manifested as spasticity, which is a velocity-dependent enhanced elongation reflex, usually accompanied by hyperreflexia of tendons and clonus. Spasm is a typical symptom of upper motor neuron injury. Its pathophysiology involves abnormal changes in the proprioceptive circuit, manifested as enhanced rather than inhibitory mutual promotion of the motor neuron pool of antagonistic muscles. In addition, the afferent fibers that inhibit reflexes after tendon stretching may be damaged, resulting in weakened inhibition. Dysfunction of the muscle spindle and Gorky tendon organs is also the core pathological basis of spasm[12]. Muscle tone hyperactivity in the lower extremities is particularly common in patients with spastic cerebral palsy, which can lead to typical "scissor gait" and foot deformities[13]. For instance, spasms of the triceps surae (gastrocnemius and soleus) can lead to increased tension in the flexor plantar muscles of the ankle, thereby affecting standing and walking functions[14].

From the performance evaluation of the model, the AUC values of the training sets are relatively high, with 0.978 for the left ankle joint training set and 0.970 for the right ankle joint training set. This indicates that the model has a strong discriminatory ability on the training data. However, the AUC values of the validation set are relatively low, with 0.631 for the left ankle joint and 0.649 for the right ankle joint, indicating that the model has overfitting and its generalization ability needs to be improved. This might be due to the relatively small sample size, which causes the model to learn the features of the training data too meticulously during the training process, including some noise and accidental factors, thus performing poorly when facing new validation data. In addition, insufficient diversity of data may also be one of the reasons for overfitting. If the feature distribution in the training data is not extensive and comprehensive enough, the model will have difficulty adapting to new data in different situations.

From the SHAP image of the left ankle joint, it can be seen that the radiomics features of five brain regions, namely the posterior part of the right internal capsule lentiform nucleus, the posterior part of the left internal capsule lentiform nucleus, the posterior radiation of the left thalamus (including visual radiation), the right occipital pole, and the anterior part of the right middle temporal gyrus, are important features for predicting muscle tone hyperactivity in the left ankle joint. The inner capsule is a key white matter area indispensable for multiple neural functions, containing important ascending and descending fiber bundles[15]. Its anatomical location is behind the lenticular nucleus and outside the thalamus, making it an important channel for information transmission between the cortex and subcortical structures. The main component of the posterior inner capsule of the lenticular nucleus is the visual radiation (also known as the geniculate fasciculate beam), which transmits visual information from the lateral geniculate body of the thalamus to the primary visual cortex of the occipital lobe[16]. In addition to the visual pathway, the posterior inner capsule of the lenticular nucleus also contains components radiating from the thalamus, including parietal pontine fibers and occipital pontine fibers[17]. These fibers connect the parietal and occipital lobes to the pons nucleus and play a role in motor control and coordination through the corticopon-cerebellar pathway[18].The thalamus, as an important relay station of the central nervous system, emits extensive projections from its nuclei to the cerebral cortex, and these projection fibers form the thalamic-cortical tracts[19]. Posterior thalamic radiation is mainly composed of projection fibers emitted by the posterior ventral nucleus of the thalamus, the lateral geniculate body and the medial geniculate body. These fibers aggregate in the posterior limbs of the inner capsule and further disperse to different regions of the cerebral cortex[20]. A study shows that posterior radiation of the right thalamus (including visual radiation) may be a sensitive imaging marker for the early identification of cognitive changes in type 2 diabetes mellitus (T2DM)[21].The Right Occipital Pole is the most posterior area of the occipital lobe of the brain. Its main function is closely related to visual processing, especially the primary visual cortex (V1, Brodman 17 area), which is mainly located in this area[22]. This area plays a core role in visual perception, spatial positioning, and early visual feature extraction (such as direction, contrast, and simple shapes), processing primary visual information from the contralateral field of vision (i.e., the left field of vision). Lesions at the right occipital pole often lead to left-side homologous hemianopia, that is, the loss of the left visual field[23].The temporal lobe is an important component of the cerebral cortex and is involved in multiple functions such as auditory processing, memory formation and emotional regulation. The middle

temporal gyrus is one of the three main gyrus of the temporal lobe, located between the superior temporal gyrus and the inferior temporal gyrus. The anterior part of the right middle temporal gyrus specifically refers to the first third of this gyrus. It plays a key role in a variety of advanced cognitive functions, especially in semantic processing, language understanding and social cognition. This area mainly corresponds to Brodman District 21 and part of District 38[24].

It can be seen from the SHAP plot of the right ankle joint that the radiomics features of brain regions such as the posterior left superior temporal gyrus, the posterior right superior temporal gyrus, and the left corticospinal tract are important features for predicting muscle tone hyperactivity in the right ankle joint. The posterior superior temporal gyrus (pSTG) of the left and right is a key component of the temporal lobe and plays an important role in advanced functions such as human language, auditory processing and social cognition[25]. Although they are anatomically symmetrical, the pSTG of the left and right hemispheres functionally shows significant lateralization[26]. The left pSTG is generally regarded as the anatomical location of the Wernicke area, which is a key region for speech comprehension. Damage to this area can lead to sensory aphasia, characterized by fluent but meaningless speech and severe auditory comprehension disorders[27].The corticospinal tract is the main descending motor pathway that connects the motor areas of the cerebral cortex with spinal cord neurons[28]. It originates from the motor areas of the cerebral cortex, and its fibers travel through the posterior limbs of the inner capsule and the ventral lower part of the brainstem to the spinal cord. It regulates the α and γ motor neurons in the anterior horn of the spinal cord through direct or indirect synaptic connections, and ultimately controls the voluntary movement of the skeletal muscles of the trunk and limbs. Previous clinical studies have shown that the degree of corticospinal tract injury is significantly positively correlated with the severity of post-stroke spasm, and the improvement of motor function in patients with post-stroke spasm is closely related to the remodeling of corticospinal tract axons[29].

It is noteworthy that the spastic state of patients with cerebral palsy is caused by pyramidal tract injury. Among the characteristics predicting muscle tone hyperactivity of the left ankle joint, the posterior part of the right inner capsule lenticular nucleus and the left left cerebral peduncle conform to the course of the corticospinal tract, which is in line with the corresponding white matter composition and pyramidal tract injury theory. The brain regions such as the right precuneus cortex, the posterior part of the right superior marginal gyrus, the anterior part of the right middle temporal gyrus, the right occipital pole, and the left insular cortex are generally related to functions such as cognition, spirit, language, learning, and vision. Among the features predicting muscle tone hyperactivity of the right ankle joint, the left inner capsule hindlimb and the left corticospinal tract are related to the pyramidal tract, while the brain regions related to the other features have no association with the pyramidal tract. Previous studies have shown that patients with cerebral palsy have different brain activation patterns and neural connection characteristics, which may be the result of maladaptive or compensatory changes in the brain networks related to motor control[30]. For instance, during physical activities, functional magnetic resonance imaging (fMRI) studies have shown that the activation of the primary motor cortex in patients with cerebral palsy is weakened, while the activation of the anterior motor cortex and auxiliary motor areas is enhanced[31]. Our study extracted features based on the Harvard-Oxford Atlas and the Johns Hopkins University atlas, both of which were based on the anatomical standard spaces of healthy populations. When it is inversely transformed to the individual space of cerebral palsy patients, although nonlinear registration is used to align as much as possible, the possible ventricular enlargement, abnormal cortical folding patterns, and variations in the course of white matter fiber tracts in cerebral palsy patients may still lead to misalignment between the map and the true boundary. This misalignment may lead to feature extraction from non-target tissues (such as including part of the cerebrospinal fluid in the gray matter) and the loss of features from "variant brain regions" that actually exist but are not defined in the map. Previous studies[32] have pointed out that children with brain injury often have significant anatomical structural variations. Traditional atlas prior methods may fail in severely deformed areas, and adaptive and spatially consistent segmentation algorithms need to be relied upon. Future research can explore the adoption of probability maps based on fiber bundles, personalized brain network partitioning, or multi-map fusion strategies (extracting features from multiple maps simultaneously and then taking the intersection or voting) to reduce the bias brought by a single map. In addition, deep learning-based automatic segmentation technology for brain injury lesions has made progress in recent years and is expected to provide more accurate anatomical definitions for individualized analysis of cerebral palsy patients[32].

In this study, it was found that the muscle tone hyperactivity of ankle in patients with cerebral palsy could be predicted without brain regions related to the pyramidal tract. It is considered that this is due to the neural plasticity and functional reorganization in the brain of patients with cerebral palsy. When the pyramidal tracts are damaged, the brain will attempt to reorganize neural connections and functions, enabling brain regions that were originally not directly related to motor control to participate in the motor regulation process, in order to make up for the functional deficiencies of the damaged brain regions. This neural plasticity offers new ideas for the treatment of cerebral palsy. We can take advantage of the brain's self-repairing and adjusting ability to promote functional remodeling between brain regions through rehabilitation training and other means, thereby improving the motor function of patients.The motor dysfunction of patients with cerebral palsy not only stems from abnormal muscle tone in individual muscles, but is also related to the alteration of muscle synergy patterns. The muscle synergy theory holds that the central nervous system simplifies motor control by combining and activating the synergy modules of multiple muscles[33]. After brain injury, this collaborative pattern may undergo reorganization, manifested as abnormal common contractions or temporal disorders. Some brain regions not directly associated with the pyramidal tract (such as the middle temporal gyrus and insular cortex) discovered in this study can predict muscle tone hyperactivity of ankle, which may be related to the higher-level regulation of motor control involving these brain regions. In addition, the brain regions discovered in this study that are not related to the pyramidal tract but can predict muscle tone hyperactivity may become new therapeutic targets. In the future, in-depth research can be conducted on these brain regions to explore whether the functional activities of these brain regions can be regulated through methods such as drugs, physical therapy or neuroregulation, thereby further improving the ankle muscle tone and motor control ability of patients with cerebral palsy.

The limitations of this study: First, this study only focuses on the construction of a predictive model for muscle tone hyperactivity of ankle in patients with cerebral palsy, and is lacking in research on increased muscle tone in other parts of children with cerebral palsy. The increase in muscle tone in different parts may be influenced by different brain regions and neural mechanisms. Studying only the ankle joint may not fully reflect the overall increase in muscle tone in patients with cerebral palsy. Secondly, the radiomics feature extraction used in the study was based on the Harvard-Oxford brain Atlas and the Johns Hopkins University atlas, both of which were proposed based on normal anatomy. However, the brain structure and function of patients with cerebral palsy are significantly different from those of normal people. Relying on normal maps may not accurately capture the true structural and functional characteristics of the brain of patients with cerebral palsy, thereby affecting the accuracy and reliability of the model. Thirdly, in terms of the validation of the predictive model, the relatively limited sample size and single-center studies have led to overfitting of the research results, making it impossible to fully test the effectiveness and stability of the model in a larger population. Fourth, this study only constructed a predictive model based on radiomics features and did not comprehensively consider other factors that might affect the increase of ankle muscle tone, such as the patient's age, the severity of the condition, and the situation of rehabilitation training. These factors may interact with the characteristics of brain regions and jointly affect the muscle tone of the ankle joint. Ignoring these factors may lead to impair explanation and predictive accuracy of the model.

Funding Information: This article was supported by “Tianshan Talents”medical and health high-level talent training plan”（TSYC202401B081）.

References

[1] Pearson TS, Pons R, Ghaoui R, et al. Genetic mimics of cerebral palsy[J]. MovDisord, 2019, 34 (5) : 625-636.

[2] Sellier E, Platt MJ, Andersen GL, et al.Decreasing prevalence in cerebral palsy: a multi-site European population-based study, 1980 to 2003[J]. Dev Med Child Neurol. 2016; 58 (1) : 85-92.

[3] Galea C, McIntyre S, Smithers-Sheedy H, Reid SM, Gibson C, et al. Cerebral palsy trends in Australia(1995-2009): a populationbased observational study[J]. Developmental Medicine&Child Neurology. 2019; 61 (2) : 186-193.

[4] Korzeniewski SJ, Birbeck G, DeLano MC, Potchen MJ, Paneth N. A systematic review of neuroimaging for cerebral palsy[J]. Journal of Child Neurology. 2008; 23 (2) : 216-227.

[5] te Velde A, Morgan C, Novak I, Tantsis E, Badawi N. Early Diagnosis and Classification of Cerebral Palsy: An Historical Perspective and Barriers to an Early Diagnosis[J]. J Clin Med. 2019; 8 (10) : 1599.

[6] Bosanquet M, Copeland L, Ware R, et al. A systematic review of tests to predict cerebral palsy in young children[J]. Dev Med Child Neurol. 2013; 55 (5) : 418-26.

[7] Tusor N, Benders M J, Counsell S J, et al. Punctate White Matter Lesions Associated With Altered Brain Development And Adverse Motor Outcome In Preterm Infants [J]. Scientific Reports, 2017, 7(1).

[8] Shi L, He Y, Yuan Z, et al. Radiomics for Response and Outcome Assessment for Non-Small Cell Lung Cancer[J]. Technol Cancer Res Treat. 2018; 17: 1533033818782788.

[9] G.Lee, H.Y.Lee, H.Park, et al. Radiomics and its emerging role in lung cancer research,imaging biomarkers and clinical management: state of the art[J]. Eur.J.Radiol. 86(2017)297–307.

[10] D.Nie, J.Lu, H.Zhang, et al. Multi-channel 3D deep feature learning for survival time prediction of brain tumor patients using multi-modal neuroimages[J]. Sci.Rep. 9(1)(2019)1103.

[11] Xie H, Ma S, Wang X, Zhang X. Noncontrast computer tomography-based radiomics model for predicting intracerebral hemorrhage expansion: preliminary findings and comparison with conventional radiological model[J]. Eur Radiol. 2020; 30 (1) : 87-98.

[12] Xu D, Wu Y, Gaebler-Spira D, et al. Neural and non-neural contributions to ankle spasticity in children with cerebral Palsy[J]. Developmental Medicine& Child Neurology, 2020, 62(9):1040–1046.

[13] Fu W, Jin B, Zhao Y, et al. Clinical study on acupuncture combined with Low-frequency electric stimulation for scissor gait in children with spastic cerebral Palsy[J].Journal of Acupuncture and Tuina Science, 2015, 13(3):150–155.

[14] Mizuno S, Sonoda S, Takeda K, et al. Effect of muscle tone on ankle kinetics during gait with Ankle-foot orthoses in persons with Stroke[J]. Topics in Stroke Rehabilitation, 2017, 24(8): 567–572.

[15] Ribas E C, Yagmurlu K, Wen H T, et al. Microsurgical anatomy of the inferior limiting insular sulcus and the temporal stem[J].Journal of Neurosurgery, 2015, 122(6): 1263-1273.

[16] Forhad C, Mohammod H, Mainul S, et al. White fiber dissection of brain; the internal capsule:a cadaveric study[J]. Turkish Neurosurgery, 2010; 20 (3) : 314-322.

[17] Cowan F M, De Vries L S. The internal capsule in neonatal Imaging[J]. Seminars in Fetal and Neonatal Medicine, 2005, 10(5):461–474.

[18] Coplan J D, Kolavennu V, Abdallah C G, et al. Patterns of anterior versus posterior white matter fractional anistotropy concordance in adult nonhuman primates: Effects of early life Stress[J]. Journal of Affective Disorders, 2016, 192:167–175.

[19] Milardi D, Quartarone A, Bramanti A, et al. The Cortico-Basal Ganglia-Cerebellar Network:Past,Present and Future Perspectives[J]. Frontiers in Systems Neuroscience. 2019, 13:61.

[20] Wiegell M R, Tuch D S, Larsson H B W, et al. Automatic segmentation of thalamic nuclei from diffusion tensor magnetic resonance Imaging[J]. NeuroImage, 2003, 19 (2) : 391-401.

[21] Wakana S, Jiang H, Nagae-Poetscher L M, et al. Fiber Tract–based Atlas of Human White Matter Anatomy[J]. Radiology, 2004, 230(1):77–87.

[22] Braddick O.Occipital Lobe(Visual Cortex): Functional Aspects[M]//International Encyclopedia of the Social& Behavioral Sciences. Elsevier, 2015:127–132.

[23] Papageorgiou E, Ticini L F, Schiefer U. Peripheral Homonymous Hemianopia[J]. Journal of Neuro-Ophthalmology, 2012, 32(1):5–12.
[24] Hung J, Wang X, Wang X, et al. Functional subdivisions in the anterior temporal lobes: A large scale meta-analytic Investigation[J]. Neuroscience& Biobehavioral Reviews, 2020, 115:134–145.
[25] Petrides M. On the evolution of polysensory superior temporal sulcus and middle temporal gyrus: A key component of the semantic system in the human Brain[J]. Journal of Comparative Neurology, 2023, 531(18):1987–1995.
[26] Joliot M, Tzourio-Mazoyer N, Mazoyer B. Intra-hemispheric intrinsic connectivity asymmetry and its relationships with handedness and language Lateralization[J]. Neuropsychologia, 2016, 93:437–447.
[27] Binder J R. The Wernicke Area[J]. Neurology, 2015, 85(24):2170–2175.
[28] HE J, ZHANG F, PAN Y, et al. Reconstructing the somatotopic organization of the corticospinal tract remains a challenge for modern tractography methods. Hum Brain Mapp. 2023; 44 (17) : 6055-6073.
[29] Cho MJ,Yeo SS,Lee SJ,Jang SH. Correlation between spasticity and corticospinal/corticoreticular tract status in stroke patients after early stage[J]. Medicine(Baltimore). 2023; 102(17):e33604.
[30] Sasikumar S, Strafella AP. The neuroimaging evidence of brain abnormalities in functional movement disorders[J]. Brain. 2021; 144 (8) : 2278-2283.
[31] Madkhali Y, Aldehmi N, Pollick F. Functional Localizers for Motor Areas of the Brain Using fMRI[J]. Comput Intell Neurosci. 2022; 2022:7589493.
[32] Pagnozzi, A. M. et al. The need for improved brain lesion segmentation techniques for children with cerebral palsy: A review. International Journal of Developmental Neuroscience 47, 229–246 (2015).
[33] SHUMAN B R, GOUDRIAAN M, DESLOOVERE K, et al. Muscle Synergy Constraints Do Not Improve Estimates of Muscle Activity From Static Optimization During Gait for Unimpaired Children or Children With Cerebral Palsy[J]. Frontiers in Neurorobotics, 2019, 13.